AD-A066 182 INDIANA UNIV AT BLOOMINGTON DEPT OF CHEMISTRY F/G 21/2
A THEORETICAL STUDY INTO THE SPATIAL DISTRIBUTION OF ATOMS SURR--ETC(U)
FEB 79 C B BOSS, G M HIEFTJE N00014-76-C-0838
UNCLASSIFIED TR-21 NL

| OF |
AD
A066 182

END
DATE
FILMED
5-79
DDC

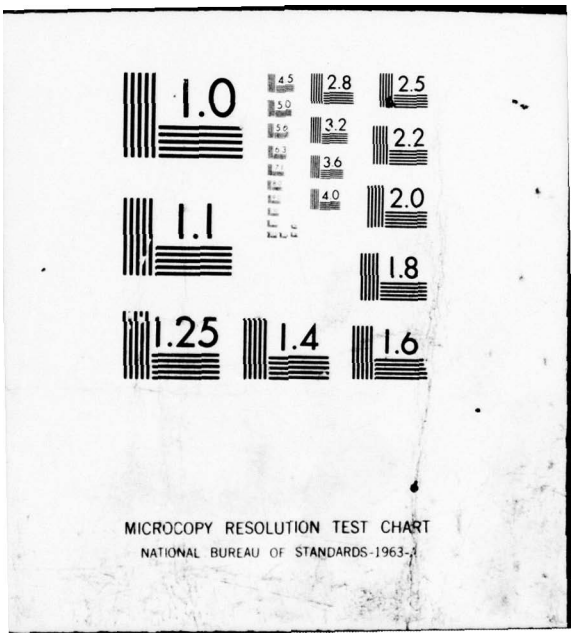
1.0
1.1
1.25
1.4
1.6
1.8
2.0
2.2
2.5
2.8
3.2
3.6
4.0
4.5
5.0
5.6
6.3
7.1
8.0
9.0
MICROCOPY RESOLUTION TEST CHART
NATIONAL BUREAU OF STANDARDS-1963-A

AD A066182

DDC FILE COPY

LEVEL II

SECURITY CLASSIFICATION OF THIS PAGE (When Data Entered)

REPORT DOCUMENTATION PAGE

READ INSTRUCTIONS BEFORE COMPLETING FORM

1. REPORT NUMBER: SIXTEEN
2. GOVT ACCESSION NO.
3. RECIPIENT'S CATALOG NUMBER: (9)

4. TITLE (and Subtitle): (6) A Theoretical Study into the Spatial Distribution of Atoms Surrounding an Individual Solute Particle Vaporizing in an Analytical Flame
5. TYPE OF REPORT & PERIOD COVERED: Interim Technical Report
6. PERFORMING ORG. REPORT NUMBER: 21

7. AUTHOR(s): (10) Charles B. Boss and Gary M. Hieftje
8. CONTRACT OR GRANT NUMBER(s): N00014-~~N14~~-76-C0838

9. PERFORMING ORGANIZATION NAME AND ADDRESS: Department of Chemistry, Indiana University, Bloomington, IN 47405 (14) TR-21, 16
10. PROGRAM ELEMENT, PROJECT, TASK AREA & WORK UNIT NUMBERS: NR 051-622

11. CONTROLLING OFFICE NAME AND ADDRESS: (15) N00014-76-C-0838
12. REPORT DATE: February 15, 1979
13. NUMBER OF PAGES: 33

14. MONITORING AGENCY NAME & ADDRESS (if different from Controlling Office): Office of Naval Research, Washington, D. C. (11) 15 Feb 79
15. SECURITY CLASS. (of this report): Unclassified
15a. DECLASSIFICATION/DOWNGRADING SCHEDULE

16. DISTRIBUTION STATEMENT (of this Report): Approved for public release; distribution unlimited (12) 33p.

17. DISTRIBUTION STATEMENT (of the abstract entered in Block 20, if different from Report): Prepared for publication in ANALYTICAL CHEMISTRY

18. SUPPLEMENTARY NOTES

DDC RECEIVED MAR 22 1979 D

19. KEY WORDS (Continue on reverse side if necessary and identify by block number): Flame Spectrometry, solute vaporization, atomic diffusion

20. ABSTRACT (Continue on reverse side if necessary and identify by block number):

A theoretical model is developed to describe the synergic effects of analyte vaporization and diffusion rates on the spatial distribution of analyte atoms in the vapor cloud surrounding an individual solute particle in a laminar flame or plasma. A mathematical convolution of the vaporization and diffusion processes is used to describe the analyte spatial distribution. Unfortunately, the resulting convolution integral cannot be solved in closed form for the experimentally observed vaporization function, and several simplifying approximations to the vaporization function are compared and shown to be useful.

DD FORM 1 JAN 73 1473 EDITION OF 1 NOV 65 IS OBSOLETE S/N 0102-014-6601

UNCLASSIFIED

SECURITY CLASSIFICATION OF THIS PAGE (When Data Entered)

176685 79 05 19 063

20. continued

With this new model, the analytical consequences of changes in both diffusion coefficient and vaporization rate are examined, and the resulting changes in spatial distribution of atoms about a typical analyte particle are compared.

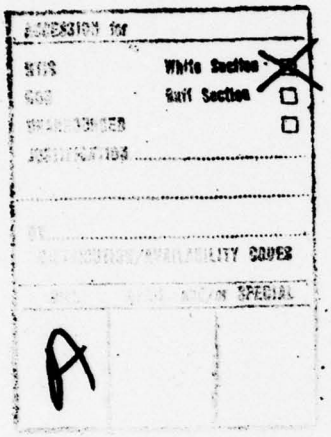

A THEORETICAL STUDY INTO THE SPATIAL DISTRIBUTION OF ATOMS SURROUNDING AN INDIVIDUAL SOLUTE PARTICLE VAPORIZING IN AN ANALYTICAL FLAME

Charles B. Boss[1]

and

Gary M. Hieftje*

Department of Chemistry

Indiana University

Bloomington, Indiana 47401

[1]Present Address: Department of Chemistry
N. C. State University
Raleigh, North Carolina 27650

BRIEF

Models are developed which describe the synergic effects of analyte vaporization and diffusion rates on the spatial distribution of atoms surrounding an individual solute particle.

ABSTRACT

A theoretical model is developed to describe the synergic effects of analyte vaporization and diffusion rates on the spatial distribution of analyte atoms in the vapor cloud surrounding an individual solute particle in a laminar flame or plasma. A mathematical convolution of the vaporization and diffusion processes is used to describe the analyte spatial distribution. Unfortunately, the resulting convolution integral cannot be solved in closed form for the experimentally observed vaporization function, and several simplifying approximations to the vaporization function are compared and shown to be useful. With this new model, the analytical consequences of changes in both diffusion coefficient and vaporization rate are examined, and the resulting changes in spatial distribution of atoms about a typical analyte particle are compared.

An important endeavor in the improvement of all atomic spectrometric methods of analysis is the study of spatial atom distributions in the analytical source. A quantitative knowledge of the physical and chemical factors that determine a particular free atom distribution is important in understanding the influence of many interferents and is an essential part of the effort to achieve absolute flame or plasma atomic spectrometric measurements (1).

The distribution of atoms in an analytical flame or plasma strongly affects the optimal experimental configuration to be employed in atomic spectrometry. For example, in flame spectrometry, an optimal flame height exists where most of the analyte atoms have been released but where they have not yet fully equilibrated through ionization or recombination reactions. In addition, the horizontal distribution of atoms across a flame or plasma determines the proper optical aperture for measurement of the atoms, be it by absorption, emission, or fluorescence. For instance, a narrow atomic spatial distribution in an atomic absorption experiment will cause greater non-linearity of working curves due to source radiation entering the detector without having passed through the sample atoms. In an atomic fluorescence experiment as well, a narrow atomic vapor cloud would experience a smaller cross-section of the exciting radiation than a broader cloud. Lastly, in atomic emission spectrometry, a high concentration of analyte atoms within a narrow region of the flame or plasma center would produce different self-absorption characteristics than those produced by the same number of atoms distributed over the entire source.

Conveniently, the same processes affect the distribution of atoms in both flames and plasmas, so that studies designed to explore these phenomena in one source will yield results applicable to the other. In both kinds of source, final spatial variations in atom concentration are governed by the

initial distribution of aerosol droplets, by the location of the dried (and perhaps fragmented) solute particles which result from desolvation of the original aerosol, and by the spreading of atomic vapor produced upon vaporization of the solute particles. In turn, localized variations in the number density of droplets, particles, and atoms are controlled by two distinguishable forces: convective and diffusive. Convective forces arise from motion of the flame or plasma gases about the droplets or particles while diffusive forces arise from concentration gradients and serve to spatially spread the droplets, particles, and atoms apart from each other. Clearly, prediction of the final atom concentration in an analytical source will require a complete understanding of the effect of both these forces on the sample components during the atomization process.

In flame atomic spectrometry, it has been established that contaminants or matrix components in nebulized solutions can cause changes in the lateral distribution of analyte atoms in the measurement region (2-4). Clearly, this kind of interference can be quite troublesome in practical flame spectrometry. For example, if a sample and standard solution create different lateral atom distributions and the spectrometer's optical system is optimized for the distribution of the standard, the sample measurement will produce either lower or higher sensitivity, depending on whether the sample atoms are more or less dispersed than those of the standard.

L'vov and co-workers (5-7) have attributed these lateral distribution anomalies to differences in the size and density of the aerosols generated from the two solutions, and a consequent change in the vertical spread of the aerosols as they emerge from the burner top. In contrast, West, Fassel, and Kniseley (8) ascribed the lateral distribution variations to an interferent-produced change in the maximum vaporization region of the analyte. In practice, either mechanism for the interference seems viable and in

most situations the two probably act in concert to determine the observed atom distributions. In order to understand how the lateral spread of aerosol particles and the vaporization rate of those particles interact to produce an observed lateral distribution of atomic vapor, and indeed to understand the detailed microscopic processes leading to atom formation and distribution, it is most meaningful to examine the spatial distribution of atoms created by an individual aerosol particle in a laminar analytical flame.

Accordingly, the objective of this paper is to develop an accurate model of the spatial distribution of atoms generated by volatilization of an individual solute particle in a laminar analytical flame. This model portrays the combined effects of vaporization and diffusion as a convolution of the two processes and neglects the influence of vapor-phase reactions on the resulting spatial atomic distributions. A rigorous numerical solution to this convolution will be presented and evaluated. In addition, approximate vaporization rate functions will be compared which allow analytical solutions to the diffusion-vaporization convolution, and which yield more readily utilizable mathematical expressions. In a paper to follow, experimental measurements will be used to verify the validity of the work and model presented herein.

THEORETICAL MODEL

As a solution droplet travels through an analytical flame, the heat transferred to it from the flame causes the solvent to evaporate (9). Once desolvation is complete, the surface temperature of the dried aerosol particle will rise and soon reach a level sufficient to cause noticeable volatilization of analyte atoms. Because these events are kinetically controlled, droplets of a particular size and which follow a particular

path through the flame will require a reproducible residence time in the flame before analyte vaporization begins (10). Correspondingly, because droplets and their vapor products travel vertically with the flame gases, any variation in the time required for desolvation will merely produce a change in the flame height where vaporization begins. Other than this predictable vertical shift, changes in droplet residence time will have little effect on the spatial distribution of atoms created by an individual aerosol droplet and will be ignored here. Accordingly, in the present model, the time when volatilization of analyte atoms first begins will be assigned the time coordinate reference $t = 0$; any displacement of this temporal reference can then be easily incorporated into further treatments.

As soon as an solution droplet is introduced into a laminar flame, the rapidly rising flame gases act through viscous forces to accelerate it; by the time the droplet is completely desolvated, its velocity is experimentally indistinguishable from that of the flame (10-12). In turn, because a dried, vaporizing solute particle travels essentially at the flame gas velocity, it can be assumed to be surrounded symmetrically by its vaporization products. Consequently, a spherical spatial coordinate system can conveniently be adopted, whose origin ($r = 0$) lies at the center of mass of the vapor cloud. Of course, because the cloud travels at or near the flame velocity, this origin is not fixed. However, by defining such a moving reference, the spherically symmetrical cloud can be described in terms of a single spatial variable r.

With the aid of this spatial and temporal coordinate system, the distribution of atoms about a volatilizing particle can be described. Analyte atoms released during the vaporization process can be carried away from the particle by either diffusion or convection. Of course, in a laminar analytical flame such as most often employed in practical flame

spectrometry, the predominant mass transfer phenomenon is diffusion. Therefore, the transport of analyte atoms within the spherical vapor cloud is governed principally by Fick's laws (13), and the radially and temporally dependent concentration of analyte atoms $C(r,t)$, will be given by:

$$\frac{\delta C(r,t)}{\delta t} = D\left[\frac{\delta^2 C(r,t)}{\delta r^2} + \frac{2}{r}\frac{\delta C(r,t)}{\delta r}\right] \qquad (1)$$

In equation 1, t is time measured from the onset of analyte vaporization, D is the diffusion coefficient, and r is the radial distance from the center of the spherical vapor cloud.

If vaporization were instantaneous, equation 1 could be solved in a rather straightforward manner. To do so, let N_t be the number of atoms vaporized; then at any time after vaporization,

$$C(r,t) = \frac{N_t}{8(\pi Dt)^{3/2}}\, e^{-r^2/4Dt} \qquad (2)$$

Unfortunately, vaporization occurs on the same time scale as does the diffusive transport of atoms. Thus, each successive increment of analyte vapor must diffuse into a region which has a concentration of analyte atoms already established by the previously vaporized analyte. Because diffusive forces are controlled by concentration gradients, the solution of Fick's Laws for this problem must account for the fact that analyte vaporization occurs during the diffusive transport process. This accounting is possible through the incorporation of a vaporization function $\Phi(t)$ into equations 1 and 2. To incorporate a vaporization function into equation 1, a solution must be found which sums the effects of each small increment of analyte vapor introduced. The solution, accounting for the synergic effects of diffusion and volatilization in creating a spatial distribution of atoms,

is a convolution and, with a generalized analyte vaporization rate, $\Phi(t)$, takes the form:

$$C(r,t) = \frac{1}{8(\pi D)^{3/2}} \int_0^{t_f} \Phi(t') \frac{e^{-r^2/4D(t-t')}}{(t-t')^{3/2}} dt' \qquad (3)$$

In this equation, t' is a delay parameter accounting for the vaporization from the beginning of vaporization (where $t = 0$) and summing the effects of each increment up to the last time to be considered (where $t = t_f$). To apply equation 3 to the calculation of atomic concentrations at different times during vaporization requires that the range of the integral (the time range under consideration) include all significant analyte vaporization; thus, t_f must be set equal to the observation time t. However, when post-vaporization times are of interest, only the vaporization period need be included in the range of the integration, so that t_f must then be set equal to the time corresponding to the completion of vaporization.

Of course, for the above treatment to accurately describe the spatial distribution of analyte atoms, an appropriate vaporization function $\Phi(t)$ must be chosen. Hieftje and Bastiaans (10) have shown experimentally, through measurement of the rate of analyte appearance from indiviual solution droplets in laminar analytical flames, that of radius of a vaporizing solute particle follows a relationship of form

$$t = \frac{1}{k}(r_o^2 - r_d^2) \qquad \text{for } 0 \le t \le \frac{r_o^2}{k} \qquad (4)$$

where r_o is the initial dry aerosol particle radius (μm), r_d the radius at time t, and k is the vaporization rate ($\mu m^2/s$). Obviously, the mass lost by the condensed-phase particle as its radius decreases must be gained by the vapor phase. Because a certain fraction, ξ, of that mass entering the

vapor phase will be in the form of free analyte atoms, the relation for the flux of atoms (atoms/s) into the vapor phase, $\Phi(t)$, can be derived:

$$\Phi(t) = 2\pi\rho\xi k(r_o^2 - kt)^{1/2} \qquad \text{for } 0 \leq t \leq r_o^2/k \qquad (5)$$

$$\Phi(t) = 0 \qquad \text{for } t > r_o^2/k \qquad (6)$$

where ρ is the density of analyte atoms (atoms/μm^3) in the condensed phase. The shape of this vaporization function is graphically presented as curve A of Figure 1.

By substituting the observed analyte vaporization rate, equation 5, into the solution of Fick's Law, (equation 3) an equation can be derived which describes the atom concentration as a function of radial distance in the vapor cloud and of time from the initiation of vaporization:

$$C(r,t) = \frac{\xi\rho k}{4\pi^{1/2}D^{3/2}} \qquad (6)$$

Unfortunately, equation 6 cannot be solved in closed form but must be evaluated numerically.

Because of the potential utility of an analytical solution to this convolution integral (equation 3), it is worthwhile to approxiate the vaporization function $\Phi(t)$ by simpler but similar functions. Two such approximations will be considered here. The first and simplest approximation to the vaporization function is one representing a constant rate of mass loss; i.e., it assumes that analyte atoms are liberated at a constant rate over the entire vaporization period:

$$\Phi(t) = k_v \qquad \text{for } 0 \leq t \leq t_v \qquad (7)$$

The solution of equation 3 using this constant vaporization model is as follows:

$$C(r,t) = \frac{k_v}{4\pi Dr} \operatorname{erfc}\left(\frac{r}{2(Dt)^{1/2}}\right) \qquad \text{for } t \le t_v$$

and

$$C(r,t) = \frac{k_v}{4\pi Dr} \operatorname{erfc}\left(\frac{r}{2(Dt)^{1/2}}\right) - \operatorname{erfc}\left(\frac{r}{2[D(t-t_v)]^{1/2}}\right) \qquad \text{for } t > t_v \tag{8}$$

A closer approximation to the experimentally observed analyte vaporization function is one in which the rate of vaporization decreases linearly with time during the entire time over which vaporization takes place. The mathematical statement of this model is as follows:

$$\Phi(t) = qt + Q \qquad \text{for } 0 \le t \le t_f \tag{9}$$

where q and Q are the slope and intercept of the linear function. A graphical comparison of the true vaporization function, equation 5, and these approximations, equations 7 and 9, is given in Figure 1. The solution of the convolution integral, equation 3, with this linear approximation to the vaporization rate, equation 9, is:

$$C(r,t) = \frac{q}{4\pi rD}\left[\left(t + \frac{Q}{q} + \frac{r^2}{2D}\right)\operatorname{erfc}\left(\frac{r}{2(Dt)^{1/2}}\right) - r\left(\frac{t}{\pi D}\right)^{1/2} e^{-r^2/4Dt}\right] \qquad \text{for } 0 \le t \le t_f$$

and

$$C(r,t) = \frac{q}{4\pi Dr}\left(\left[t + \frac{Q}{q} + \frac{r^2}{2D}\right]\left[\operatorname{erfc}\left(\frac{r}{2(Dt)^{1/2}}\right) - \operatorname{erfc}\left(\frac{r}{2[D(t-t_f)]^{1/2}}\right)\right] - \frac{r}{(\pi D)^{1/2}}\left[(t-t_f)^{1/2} e^{-r^2/4D(t-t_f)} - t^{1/2} e^{-r^2/4Dt}\right]\right) \qquad \text{for } t > t_f \tag{10}$$

RESULTS AND DISCUSSION

The equations developed in the preceeding section, describing the spatial distribution of atoms surrounding a volatilizing solute particle, are sufficiently complicated that an understanding of their physical relevance cannot be gleaned by simple inspection. Moreover, a simple graph of radial concentration of analyte at any particular time is difficult to interpret. Discerning from such a plot the total number of atoms in a particular vapor cloud is not simple; one must integrate the product of the graph's value times a factor representing the volume of a standard (fixed thickness) spherical shell at each radius. Another problem with this type of graph is that the model employed here requires that the concentration of vapor phase analyte be infinite at the center of the vapor cloud during analyte volatilization. This problem derives from the fact that the vapor phase atoms are being injected into the system in an infinitely small volume.

A better appreciation for the mathematical model can be gained by plotting the number of atoms contained in a thin spherical shell of uniform thickness as a function of the shell's radial distance from the origin. Let the thickness of the shell be $\underline{\Delta r}$, and let the shell extend in radial distance from the center of the vapor cloud between $r - \Delta r/2$ and $r + \Delta r/2$. The volume of this spherical shell (ΔV) can be expressed as

$$\Delta V = 4\pi r^2 \Delta r + \pi(\Delta r)^3/3 \qquad (11)$$

The relationship between concentration and the number of atoms in the thin shell now becomes

$$N(r,t) = \Delta V\, C(r,t) \qquad (12)$$

The parameter $\underline{\Delta r}$ will be fixed for any given representation and must be

chosen on the basis of the resolution desired. A plot of N(r,t) versus radial distance in the vapor cloud can now easily be used to determine the number of atoms in a sphere of a certain size, or indeed in the entire vapor cloud, simply by observing the area under the curve from the origin to the radius desired. A plot of equation 12 reveals that $\underline{N(r,t)}$ approaches zero as the radius of the shell becomes small. This behavior does not imply that concentrations are not great near the origin; rather, the volume of the shells near the origin are simply so small that very few total atoms reside in each, even at high atom concentrations.

To evaluate the utility of the models described in the previous section, let us theoretically examine the spatial distribution of atoms predicted from a typical aerosol droplet used in a practical analytical situation. Let this average droplet be 10 μm in diameter and be comprised of an aqueous solution containing 100 μg/ml of Ca as the chloride and be vaporized in an air/C_2H_2 flame. When desolvation of this droplet is complete it can be assumed that the resulting aerosol particle will be a sphere of $CaCl_2$ of radius r_o = 0.253 μm and density $\rho = 1.167 \times 10^{10}$ Ca atoms/μm^3 (14) and which travels essentially at the flame's velocity. When this particle vaporizes, it is expected to produce a cloud of atoms whose spatial characteristics change with time in accordance with equations 6 and 12. However, two parameters, the vaporization constant and the diffusion coefficient, need to be defined in order to evaluate these equations. Bastiaans and Hieftje (12) have shown experimentally that Ca vaporizes in an air/C_2H_2 flame according to equation 5 and that the vaporization constant $\underline{k}$ is 1148 $\mu m^2 s^{-1}$. Snellman (15) has measured the diffusion coefficient of Ca in an air/C_2H_2 flame and found $D = 3.0 \times 10^8$ $\mu m^2 s^{-1}$. Figure 2 shows a three-dimensional plot of the predicted atomic population per shell, $\underline{N(r,t)}$, versus the shell's radial distance from the origin of the vapor cloud and versus time for this typical droplet in an air/C_2H_2 flame.

In calculating Figure 2, it is assumed that height in the flame is proportional to time because the aerosol particle and its volatilization products move at the flame's velocity. At a typical rise velocity for an air/C_2H_2 flame of 10 m/s (12,16,17), one millisecond of elapsed time represents an upward translation of one centimeter for the center of the vapor cloud. Consequently, for the particle under consideration, vaporization occurs during the first 55.8 μs, during which time the cloud and particle move upward 0.558 mm. Figure 2 shows that during this vaporization time, the number of liberated analyte atoms increases while the diffusive forces spread the vapor cloud radially. After the completion of vaporization, the number of atoms in the cloud remains constant but diffusion continues to spread the vapor cloud.

The results portrayed in Figure 2 are not unexpected. However, of greater interest is what happens to the analyte vapor cloud when a matrix component causes a change in the analyte volatilization rate. In the mathematical models proposed here, vaporization is an important factor in determining the spatial distribution of analyte atoms. To underscore this fact, Figure 3 depicts the differences in the time-varying atomic spatial distribution which would result if only the vaporization rate of the particles should change. Figures 3a, b, c, and d represent radial atomic populations for 10 μs, 50 μs, 70 μs, and 200 μs after the initiation of analyte volatilization respectively. In each instance curve A represents the number of atoms per shell (shell width, Δr, is 100 μm for the same "typical" $CaCl_2$ solution droplet used to calculate Figure 2. The curves labeled B and C represent similar calculations for the same solution droplet but with a different vaporization rate being assumed. Specifically, curves B and C represent a 20% change (slower and faster respectively) in the analyte vaporization rate.

In Figure 3a, one sees that the major initial effect of changing the vaporization rate constant is that the total number of atoms present in the vapor phase is altered. This conclusion derives from the different areas but similar shapes of the three curves in Figure 3a. For example, comparing the areas of curves A and B in Figure 3a, one calculates for this particular system that a particle with a 20% slower vaporization rate (curve B) yields about 20% fewer freed analyte atoms after 10 μs. In comparison, Figure 3b shows similar differences in the number of atoms for the three vaporization rates near the end of the vaporization process. By this time, 50 μs after the start of analyte volatilization, subtle differences in the shapes of the vapor clouds begin to appear. The apparent trend is for the more slowly vaporized analyte to form a more compact vapor cloud. This trend is more dramatically shown in Figure 3c, where analyte volatilization is complete even for the slowest case being considered. In Figure 3c, curves A, B, and C have equal areas, indicating that there are equal numbers of atoms in the vapor phase after volatilization is complete. On the other hand, curve B is considerably shifted toward the origin, demonstrating that slowed vaporization of analyte causes the resulting vapor cloud to be less diffuse. Figure 3d illustrates that at a relatively long time after the completion of vaporization, the effects caused by small changes (± 20%) in the analyte vaporization rate are still present although of lesser magnitude than earlier in the cloud's history.

In contrast to the changes wrought by an altered vaporization rate (Figure 3), Figure 4 reveals the effects of changing analyte diffusion coefficient on its distribution in the vapor cloud. The curves labeled A in Figure 4 are again the predicted time-varying atomic spatial distributions for the same "typical" $CaCl_2$ solution droplet used in Figures 2 and 3. In all cases, curves labeled D and E represent a 20% decrease and

increase, respectively, in the diffusion coefficient from the standard $CaCl_2$ solution droplet plotted in curves A. Figures 4a, b, c, and d represent the distribution of the vapor-phase Ca after 10 μs, 50 μs, 70 μs, and 200 μs, respectively, from the start of analyte vaporization. In contrast to Figure 3, at every time being considered here, curves A, D, and E have equal areas, indicating that the vapor clouds being represented contain an equal number of atoms. As expected, at each selected time, the general shape of curves A, D, and E are similar. Curve D, with its more mobile atoms, consistently displays a more diffuse vapor cloud.

Thus, it appears that both vaporization rate and diffusion coefficient are important factors in determining the spatial distribution of analyte atoms in a flame. However, the effects of the two factors are distinguishable. One difference in the effects is apparent during the analyte vaporization period, i.e., before the time when vaporization is complete. Figures 3a and 3b show that when vaporization rates differ, the total number of atoms present at any one time during vaporization will also differ. On the other hand, Figures 4a and 4b show that if diffusion coefficients change, only the spread of atoms and not their number will change at a particular time during volatilization.

Figures 3d and 4d show that at long times after analyte volatilization is complete, another difference exists between the effects of changing vaporization rates and changing diffusion coefficients. The variation in spatial spread of atoms caused by alterations in analyte volatilization rate become relatively small, as seen in Figure 3d. In contrast, the dependence of atomic distribution on vapor-phase analyte mobilities can be seen in Figure 4d to be still relatively large. At intermediate times the effects of the two changes are very similar, as can be seen by comparison of Figures 3c and 4c.

Because the spatial distribution of atoms is controlled by both the diffusion coefficient and the vaporization rate, the mechanism for any "lateral diffusion interference" might result from changes in either or both. However, in conventional flame systems, it will be difficult to ascribe the observed interference to either source. While differences in these effects seem dramatic in Figures 3 and 4, the unpredictability and lack of control of typical nebulizers and burners makes it unlikely that the effects of diffusion and vaporization will be distinguishable from each other. The differences noted during vaporization would require optical resolution on the order of hundreths of millimeters in a conventional flame system. Other differences, noted in Figures 3 and 4 long after particle volatilization is complete, would also be difficult to observe in typical analytical flames. Such observations would have to be made high in the flame, where the flame is unstable and where atmospheric entrainment becomes significant.

Convenient incorporation of the foregoing theory into models for atom formation and into studies on interference effects requires a closed-form solution to the integral equations; in turn, such closed-form solutions require approximations to the vaporization function $\Phi(t)$ to be employed. Because equations 8 and 10 represent such approximate solutions, let us evaluate how well they represent the true (equation 6, numerically integrated) behavior under a variety of conditions and which would be best to employ in further treatments. In the constant vaporization (CV) model, the vaporization rate, k_v, and vaporization period, t_v, can be varied to produce the best fit to the true vaporization characteristics of the analyte, represented by equation 5 and portrayed in curve A of Figure 1. The best fit is found by keeping t_v equal to the true function's vaporization period, r^2_o/k. Requiring that both vaporization functions produce the same number

of atoms sets the value of the vaporization rate, $\underline{k_v}$. In the case of the 10 μm droplet of $CaCl_2$ used in Figures 2 through 4, a best fit of the CV model to the true, experimentally confirmed vaporization function is:

(13)

In the linear vaporization model (LV), three parameters are available to adjust the approximate vaporization function: q, Q, and t_f. The values of these parameters are determined by minimizing the integral of the square of the difference between the true and approximate functions. This model best fits the experimentally determined vaporization of the 10 μm droplet of $CaCl_2$ when:

(14)

Figure 1 graphically compares the true, experimentally confirmed vaporization function with these two approximations, represented by equations 13 and 14.

Using the above approximations to the vaporization function, Figure 5 compares the constant vaporization (CV) and the linear vaporization (LV) models to the behavior predicted by the more rigorous theory of equation 6. Figure 5a portrays the atomic spatial distributions predicted for 10 μs after the initiation of analyte volatilization. Both LV and CF approximations predict the correct shape for the atomic vapor cloud at this very early time, even though the CV model fails to predict the correct number of atoms in the vapor cloud. Figure 5b shows that near the end of vaporization the constant vaporization model more closely predicts the correct number of atoms in the vapor cloud but the atoms are decidedly closer to the origin than the true function indicates; at this same time, the linear vaporization function fits the true behavior very well indeed. Figure 5c shows that shortly after the

completion of vaporization the linear vaporization model is indistinguishable from the numerical integration of equation 6 while the constant vaporization model predicts a considerably smaller vapor cloud. A relatively long time after the completion of vaporization, portrayed in Figure 5b, both the constant and linear vaporization models provide a reasonable approximation to the true predicted behavior. Thus it appears that the linear vaporization model, represented by equation 10, can be used to reasonably approximate atomic distribution in a large number of instances while the constant vaporization model only approximates the spatial atomic distributions at long times after vaporization is complete.

CONCLUSIONS

The spatial distribution of atoms created by the vaporization of a single aerosol particle in a laminar flame can be mathematically modeled. Equation 3 is the general mathematical representation of this model. A rigorous solution of the model, using an experimentally determined vaporization rate, requires numerical integration of equation 6. The results of this integration have been used to prove that the rate of volatilization does indeed play a significant role in determining the spatial distribution of atoms in an individual vapor cloud.

The theory of spatial distribution of analyte atoms vaporized from individual aerosol droplets, as presented here, distinguishes between the effects of analyte mobility and vaporization. For this reason, these theories should be useful in determining the mechanism of the "lateral diffusion" interferences in practical flame atomic absorption spectrometry.

Coupled with a prediction of the distribution of aerosol droplets entering a practical flame, this theory should aid in predicting the spatial distribution of atoms in even complex flame systems (18). Such accurate

descriptions of analyte distributions will be essential in the quest to achieve absolute flame atomic absorption measurements.

In some applications of this theory, an equation which does not require numerical integration may be desirable. Such analytical solutions are provided by equations 8 and 10 through the use of approximations to the vaporization rate. While these solutions are not as rigorous as equation 6, the error they cause under various conditions has been evaluated. The linear vaporization model, equation 10, can be used to reasonably approximate atomic distributions both during and after analyte vaporization. While the constant vaporization model, equation 8, never predicts spatial distributions as accurately as the linear model, the errors become small at long times after vaporization. For some applications, the relative mathematical simplicity of equation 8 may be more important than the errors that its use will cause.

Of course, the calculation of spatial atomic distributions for any particular system requires a knowledge of the analyte diffusion coefficient and vaporization rate. Bastiaans and Hieftje (12) and Clampitt and Hieftje (19) have experimentally studied rates of analyte vaporization in flames. The diffusion rates of atoms in flames have been measured by several investigators (15,20).

The theory, as presented here, is limited in that it does not account for perturbations in the atomic vapor cloud shape due to the overlap of vapor clouds from neighboring aerosol particles. This theory also does not account for the effects of chemical reactions which may change the free atomic populations in different portions of the vapor cloud.

In a subsequent publication (21), this theory will be tested with experimentally measured spatial distributions of analyte vaporized from individual solution droplets injected into an analytical flame. These measurements will be used to deduce effective analyte diffusion coefficients and investigate the lateral diffusion interference.

References

1. B. V. L'vov, D. A. Katskov, L. P. Kruglikova, and L. K. Polzik, Spectrochim. Acta, Part B, 31, 49 (1975).

2. S. R. Koirtyohann and E. E. Pickett, Anal. Chem., 40, 2068 (1968).

3. A. C. West, V. A. Fassel, and R. N. Kniseley, Anal. Chem., 45, 1586 (1973).

4. J. B. Willis, Spectrochim. Acta, Part B, 25, 487 (1970).

5. B. V. L'vov, L. P. Kruglikova, L. K. Polzik, and D. A. Katskov, J. Anal. Chem. USSR, 30, 545 (1975).

6. B. V. L'vov, L. P. Kruglikova, L. K. Polzik, and D. A. Katskov, J. Anal. Chem. USSR, 30, 551 (1975).

7. B. V. L'vov, L. P. Kruglikova, L. K. Polzik, and D. A. Katskov, J. Anal. Chem. USSR, 30, 709 (1975).

8. A. C. West, V. A. Fassel, and R. N. Kniseley, Anal. Chem., 45, 2420 (1973).

9. N. C. Clampitt and G. M. Hieftje, Anal. Chem., 44, 1211 (1972).

10. C. B. Boss and G. M. Hieftje, Anal. Chem., 49, 2112 (1977).

11. G. M. Hieftje and H. V. Malmstadt, Anal. Chem., 40, 1860 (1968).

12. C. J. Bastiaans and G. M. Hieftje, Anal. Chem., 46, 901 (1974).

13. H. S. Carslaw and J. C. Jaeger, Conduction of Heat in Solids, 2nd edition, Clarendon Press, Oxford, England (1959).

14. Calculated from Handbook of Chemistry and Physics, 54th Edition, R. C. Weast, ed., CRC Press, Cleveland, Ohio, pp. 13-77 (1973).

15. W. Snellman, Ph.D. thesis, University of Utrecht, 1965.

16. T. Hollander, Ph.D. thesis, University of Utrecht, 1964.

17. C. B. Boss and G. M. Hieftje, Appl. Spectrosc., 33, 377 (1978).

18. K-P. Li, Anal. Chem., 48, 2050 (1976).

19. N. C. Clampitt, Jr., Ph.D. thesis, Indiana University, 1974.

20. K Kitagawa and T. Takeuchi, Anal. Chim. Acta, 67, 457 (1973).

21. C. B. Boss and G. M. Hieftje, Anal. Chem., in preparation 1978.

vapor introduced. The solution, accounting for the synergic effects of diffusion and volatilization in creating a spatial distribution of atoms,

GLOSSARY

$C(r,t)$	concentration of analyte atoms in the vapor phase
CV	constant vaporization model
k	vaporization rate constant for analyte atoms
k_v	vaporization rate for the constant vaporization model
LV	linear vaporization model
N	number of vapor phase analyte atoms in a spherical shell of thickness Δr
N_t	total number of vapor phase analyte atoms in a single vapor cloud.
q	slope of linear vaporization model
Q	intercept of linear vaporization model
r	distance from the center of the atomic vapor cloud
r_d	time dependent radius of the vaporizing analyte particle
r_o	initial radius of the completely desolvated aerosol particle
Δr	thickness of a spherical shell within an atomic vapor cloud
t	time, measured from the onset of analyte vaporization
t_f	integration limit for convolution
t_v	time for completion of particle vaporization
t'	delay parameter used in the convolution integral
ΔV	volume of a spherical shell of atomic vapor
$\Phi(t)$	vaporization function (atoms/s) for analyte atoms
ρ	density of analyte atoms (atoms/μm^3) in the condensed phase
ξ	fraction of the vapor phase analyte atoms which are neither bonded to other atoms or ionized.

FIGURE CAPTIONS

Figure 1. Experimentally verified and approximate models for volatilization of $CaCl_2$ in an air-acetylene flame. Curve A shows the rate of volatilization of Ca atoms from a sphere of $CaCl_2$ density $\rho = 1.16 \times 10^{10}$ Ca atoms/μm^3, having an initial dry radius $r_o = 0.253$ μm and vaporizing in an air-acetylene flame according to equation 5. Vaporization constant is $k = 1148$ μm^2 s^{-1}. Reference point of the time axis, $t = \emptyset$, is the initiation of Ca volatilization. Curve CV is the flux of Ca atoms into the vapor phase predicted for the same physical system by the constant vaporization model, equation 13. Curve LV is the approximation to the experimentally confirmed volatilization of Ca atoms, curve A, by the linear vaporization model, equation 14.

Figure 2. Radial and time dependent vapor-phase Ca atom populations. The population of vapor-phase Ca atoms in spherical shells of uniform thickness, $\Delta r = 100$ μm is plotted with respect to the distance from the center of the vapor cloud to the spherical shell and with respect to time. The time reference point, $t = o$, is set at the onset of Ca atom vaporization. The hypothetical aerosol droplet which produced this distribution of vapor-phase Ca atoms was a 10 μm diameter droplet containing 100 μg/ml Ca as $CaCl_2$. After desolvation, vaporization of Ca was calculated according to equation 4 with $k = 1148$ μm^2 s^{-1} and is shown graphically in Figure 1. Ca vaporization is complete after first 55.8 μs plotted. The synergic effects of vaporization rate and Fick's Law diffusion, $D = 3.0$ cm^2/s, in creating the spatial distribution of atoms shown above is given in mathematical form in equation 6.

Figure 3. Changes in analyte spatial distribution caused by changes in particle volatilization rate. Curves labeled A represent the Ca atoms in a 100 μm thickness spherical shells from the same aerosol droplet assumed for Figures 1 and 2. Radial populations are predicted by the combination of equations 6 and 12. Curves labeled B and C are Ca atom populations produced from identical

droplets, but the droplet in B vaporizes 20% more slowly, and C vaporizes 20% more rapidly than the droplet in A. The effects of vaporization rate changes vary with time. Parts a, b, c, and d of this figure represent, respectively, 10 μs, 50 μs, 70 μs, and 200 μs after the initiation of Ca volatilization. Note differences in both horizontal and vertical scale in parts a, b, c, and d.

Figure 4. Changes in analyte spatial distribution caused by changes in its diffusion coefficient. The curves labeled A represent the Ca atoms in 100 μm thick spherical shells from the same aerosol droplet used in Figures 1 and 2 and the curves labeled A in Figure 3. The curves labeled D and E represent system identical to that used for curve A with only the increase and decrease, respectively, in the diffusion coefficient. The relative magnitude of the change in the diffusion coefficient is identical to the relative magnitude of the change in vaporization rate used in Figure 3 (i.e., 20%). Parts a, b, c, and d represent the radial analyte population at 10 μs, 50 μs, 70 μs, and 200 μs after the start of Ca vaporization. Note scale changes in different figures.

Figure 5. Comparison of the predicted radial analyte population produced by the use of approximate vaporization functions. The curves labeled A represent calculations identical to those of Figure 2 and curves A of Figures 3 and 4. The curves labeled CV represent the constant vaporization approximation to this model (cf. equations 8, 12, and 13). The curves labeled LV represent the linear vaporization approximation to this model used for the curves A (cf. equations 10, 12, and 14). The differences in the vaporization rates of these three models are displayed graphically in Figure 1.

originals as Fig 1

Figure 2

55

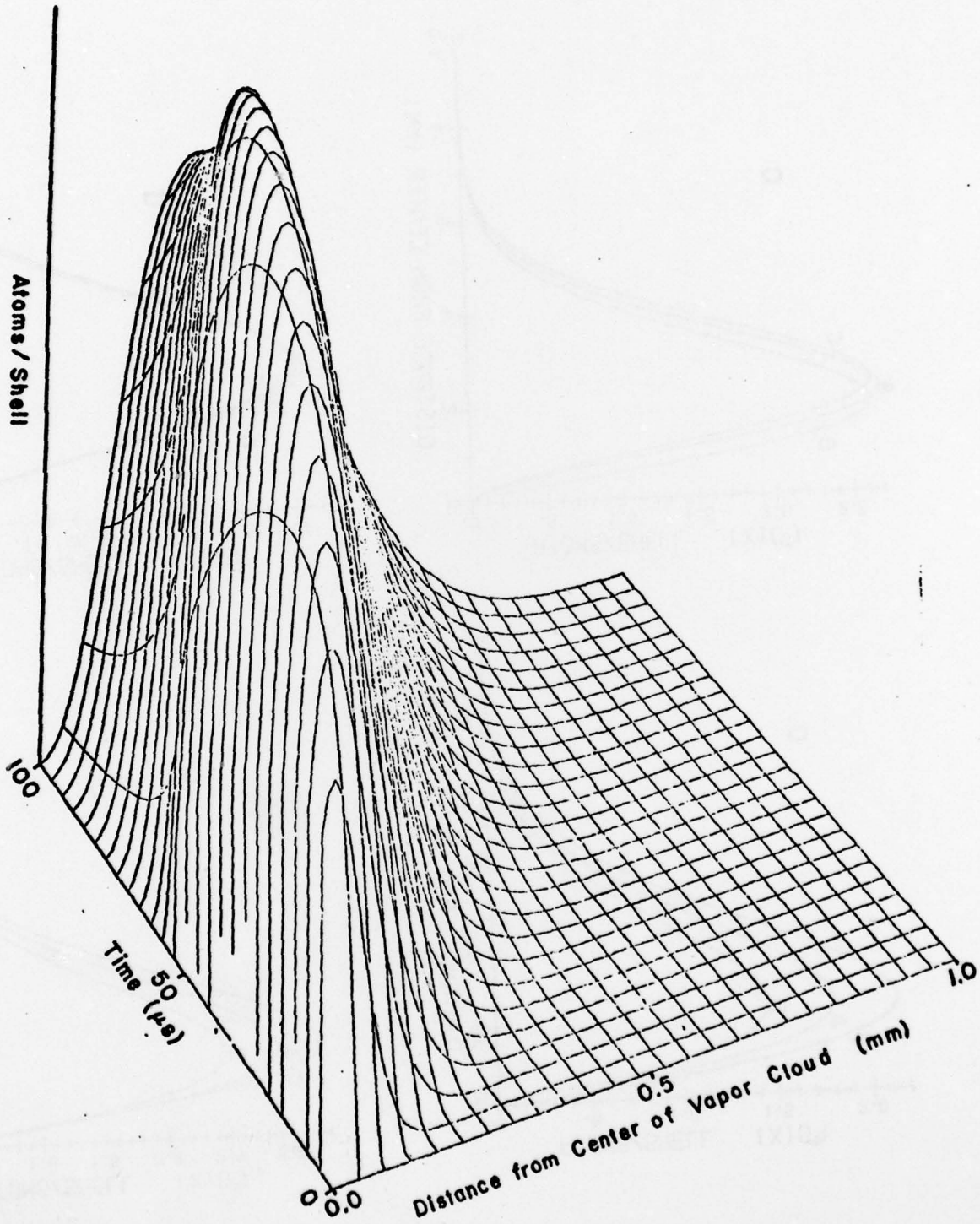
Atoms / Shell
100
0
Time (μs)
50
0.0
0.5
1.0
Distance from Center of Vapor Cloud (mm)

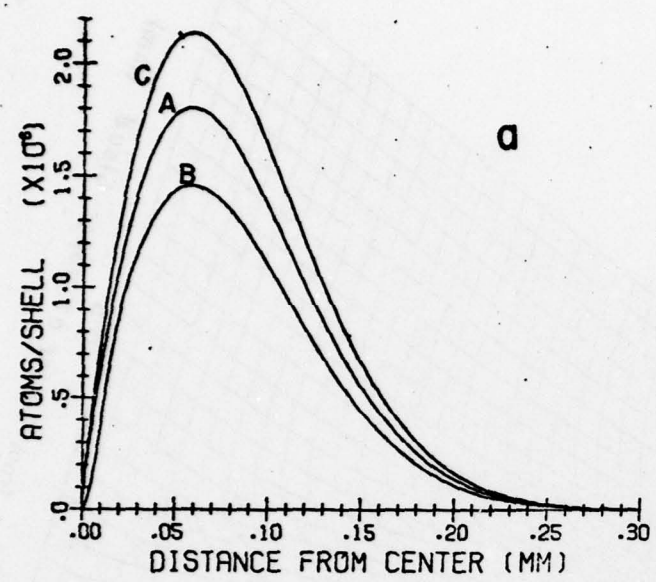
a
C
A
B
ATOMS/SHELL (X10⁶)
0.0
.5
1.0
1.5
2.0
.00
.05
.10
.15
.20
.25
.30
DISTANCE FROM CENTER (MM)

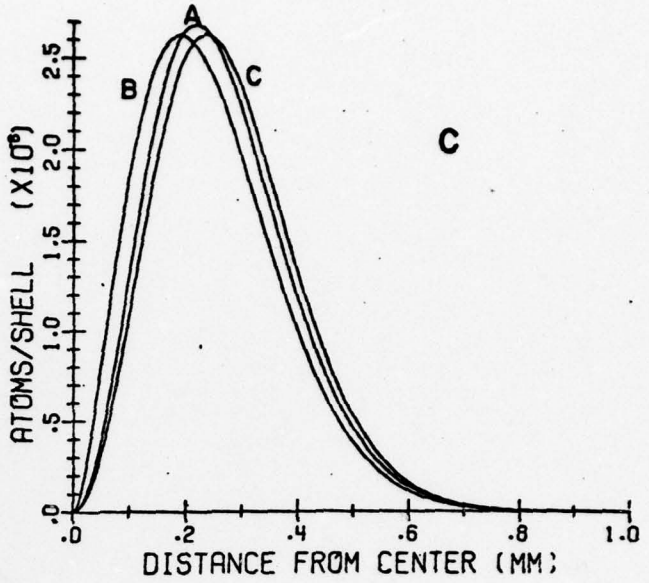
c
A
B
C
ATOMS/SHELL (X10⁶)
0.0
.5
1.0
1.5
2.0
2.5
.0
.2
.4
.6
.8
1.0
DISTANCE FROM CENTER (MM)

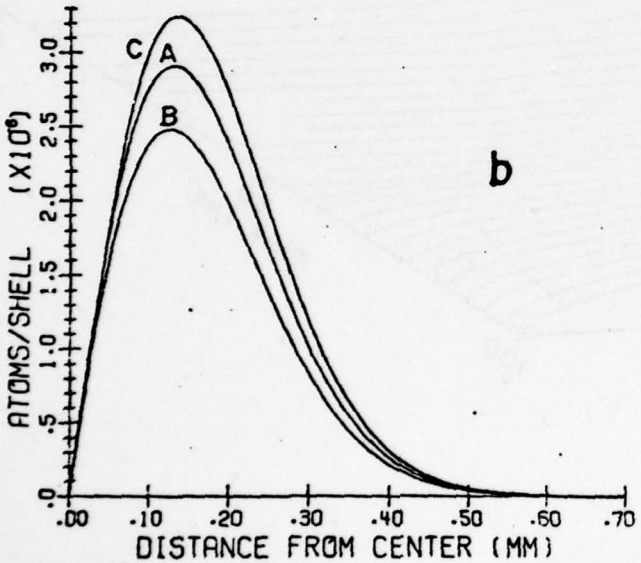
b
C
A
B
ATOMS/SHELL (X10⁶)
0.0
.5
1.0
1.5
2.0
2.5
3.0
.00
.10
.20
.30
.40
.50
.60
.70
DISTANCE FROM CENTER (MM)

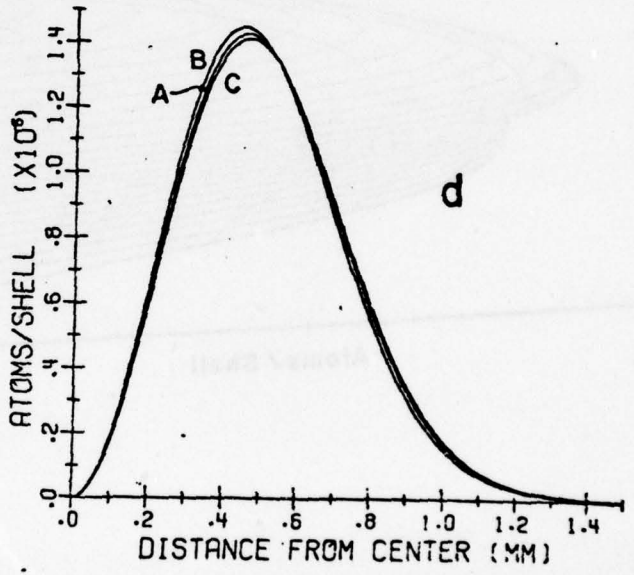
d
B
A
C
ATOMS/SHELL (X10⁶)
0.0
.2
.4
.6
.8
1.0
1.2
1.4
.0
.2
.4
.6
.8
1.0
1.2
1.4
DISTANCE FROM CENTER (MM)

Figure 3

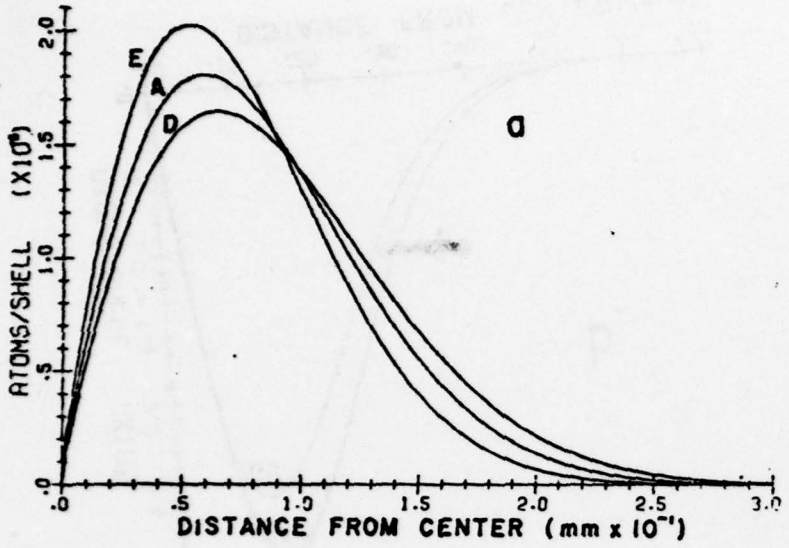
a
E
A
D
ATOMS/SHELL (X10⁶)
DISTANCE FROM CENTER (mm x 10⁻¹)

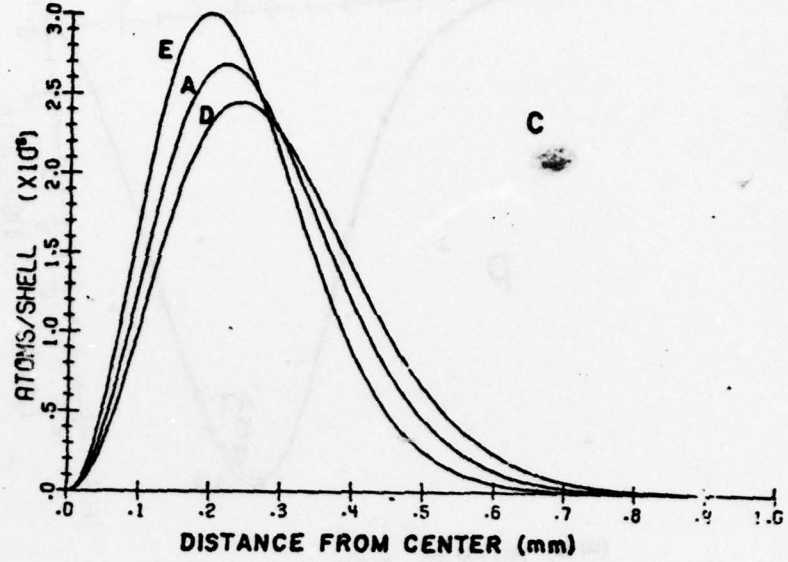
c
E
A
D
ATOMS/SHELL (X10⁶)
DISTANCE FROM CENTER (mm)

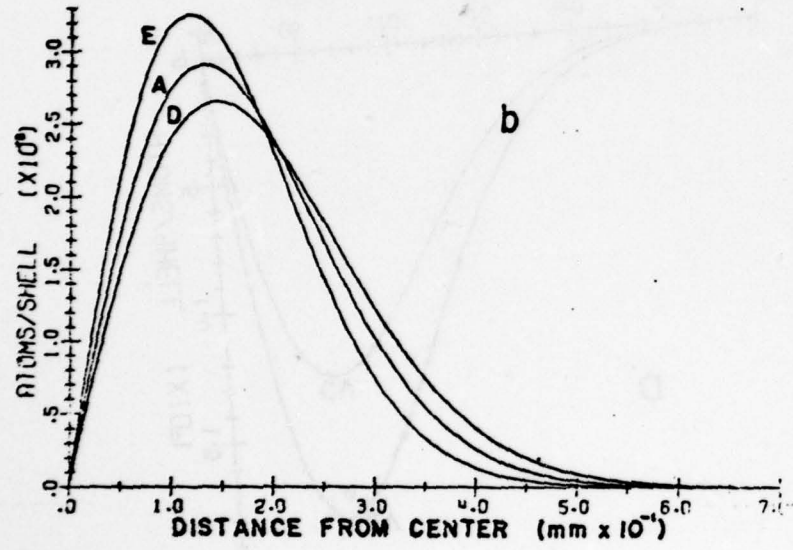
b
E
A
D
ATOMS/SHELL (X10⁶)
DISTANCE FROM CENTER (mm x 10⁻¹)

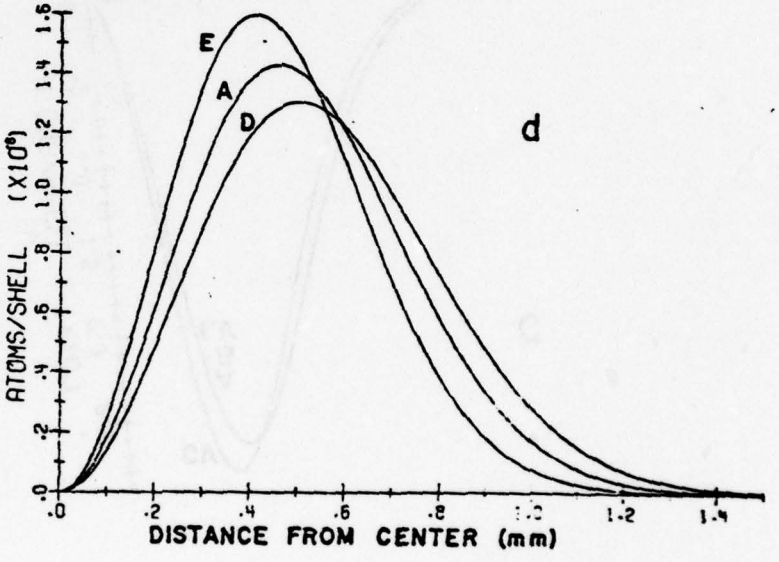
d
E
A
D
ATOMS/SHELL (X10⁶)
DISTANCE FROM CENTER (mm)

Figure 4

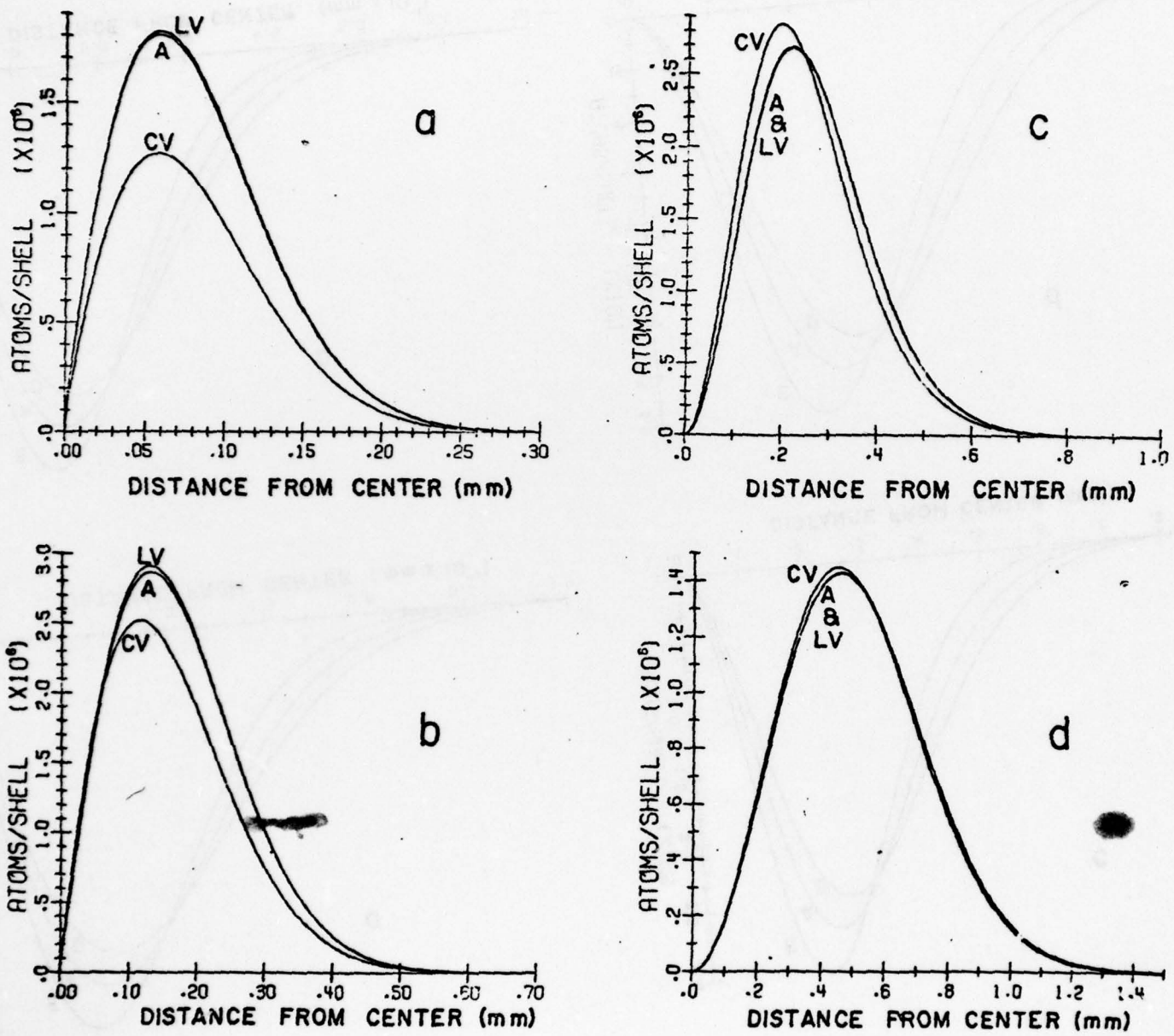
a
LV
A
CV
ATOMS/SHELL (X10⁶)
DISTANCE FROM CENTER (mm)
b
LV
A
CV
ATOMS/SHELL (X10⁶)
DISTANCE FROM CENTER (mm)
c
CV
A
&
LV
ATOMS/SHELL (X10⁶)
DISTANCE FROM CENTER (mm)
d
CV
A
&
LV
ATOMS/SHELL (X10⁶)
DISTANCE FROM CENTER (mm)

FIGURE 5

472:GAN:716:t
78u472-608

TECHNICAL REPORT DISTRIBUTION LIST, GEN

	No. Copies
Office of Naval Research 800 North Quincy Street Arlington, Virginia 22217 Attn: Code 472	2
ONR Branch Office 536 S. Clark Street Chicago, Illinois 60605 Attn: Dr. George Sandoz	1
ONR Branch Office 715 Broadway New York, New York 10003 Attn: Scientific Dept.	1
ONR Branch Office 1030 East Green Street Pasadena, California 91106 Attn: Dr. R. J. Marcus	1
ONR Area Office One Hallidie Plaza, Suite 601 San Francisco, California 94102 Attn: Dr. P. A. Miller	1
ONR Branch Office Building 114, Section D 666 Summer Street Boston, Massachusetts 02210 Attn: Dr. L. H. Peebles	1
Director, Naval Research Laboratory Washington, D.C. 20390 Attn: Code 6100	1
The Assistant Secretary of the Navy (R,E&S) Department of the Navy Room 4E736, Pentagon Washington, D.C. 20350	1
Commander, Naval Air Systems Command Department of the Navy Washington, D.C. 20360 Attn: Code 310C (H. Rosenwasser)	1
Defense Documentation Center Building 5, Cameron Station Alexandria, Virginia 22314	12
U.S. Army Research Office P.O. Box 1211 Research Triangle Park, N.C. 27709 Attn: CRD-AA-IP	1
Naval Ocean Systems Center San Diego, California 92152 Attn: Mr. Joe McCartney	1
Naval Weapons Center China Lake, California 93555 Attn: Dr. A. B. Amster Chemistry Division	1
Naval Civil Engineering Laboratory Port Hueneme, California 93401 Attn: Dr. R. W. Drisko	1
Professor K. E. Woehler Department of Physics & Chemistry Naval Postgraduate School Monterey, California 93940	1
Dr. A. L. Slafkosky Scientific Advisor Commandant of the Marine Corps (Code RD-1) Washington, D.C. 20380	1
Office of Naval Research 800 N. Quincy Street Arlington, Virginia 22217 Attn: Dr. Richard S. Miller	1
Naval Ship Research and Development Center Annapolis, Maryland 21401 Attn: Dr. G. Bosmajian Applied Chemistry Division	1
Naval Ocean Systems Center San Diego, California 91232 Attn: Dr. S. Yamamoto, Marine Sciences Division	1

Encl 1

TECHNICAL REPORT DISTRIBUTION LIST, 051C

	No. Copies
Dr. M. B. Denton University of Arizona Department of Chemistry Tucson, Arizona 85721	1
Dr. R. A. Osteryoung Colorado State University Department of Chemistry Fort Collins, Colorado 80521	1
Dr. B. R. Kowalski University of Washington Department of Chemistry Seattle, Washington 98105	1
Dr. S. P. Perone Purdue University Department of Chemistry Lafayette, Indiana 47907	1
Dr. D. L. Venezky Naval Research Laboratory Code 6130 Washington, D.C. 20375	1
Dr. H. Freiser University of Arizona Department of Chemistry Tuscon, Arizona 85721	
Dr. Fred Saalfeld Naval Research Laboratory Code 6110 Washington, D.C. 20375	1
Dr. H. Chernoff Massachusetts Institute of Technology Department of Mathematics Cambridge, Massachusetts 02139	1
Dr. K. Wilson University of California, San Diego Department of Chemistry La Jolla, California 92037	1
Dr. A. Zirino Naval Undersea Center San Diego, California 92132	1
Dr. John Duffin United States Naval Postgraduate School Monterey, California 93940	1
Dr. G. M. Hieftje Department of Chemistry Indiana University Bloomington, Indiana 47401	1
Dr. Victor L. Rehn Naval Weapons Center Code 3813 China Lake, California 93555	1
Dr. Christie G. Enke Michigan State University Department of Chemistry East Lansing, Michigan 48824	1
Dr. Kent Eisentraut, MBT Air Force Materials Laboratory Wright-Patterson AFB, Ohio 45433	1
Walter G. Cox, Code 3632 Naval Underwater Systems Center Building 148 Newport, Rhode Island 02840	1